

**Separation of an upwelling current bounding the Juan  
de Fuca Eddy, off Vancouver Island**

**Jody M. Klymak<sup>1</sup>and Everyone**

<sup>1</sup>School of Earth and Ocean Sciences and Department of Physics & Astronomy, University of Victoria,  
B.C. Canada

**Key Points:**

- The shelfbreak current along Vancouver Island separates downstream of a submarine bank.
- Offshore water is drawn onto the shelf and forms a sharp semi-persistent front with the Juan de Fuca eddy.
- The Juan de Fuca eddy shows evidence of long residence times, and little evidence of deep-water origin.

13 **Abstract**14 **Plain Language Summary**

15 The southern Vancouver Island continental shelf is very productive due to high nutrient  
 16 input from the Strait of Juan de Fuca and Salish Sea estuarine system, and substantial cross-  
 17 shelf transport due to the complicated topography. The estuarine water flows poleward,  
 18 hugging the coast as the Vancouver Island Coastal Current, and in the summer shelf water  
 19 flows equatorward. Trapped between these two currents is the Juan de Fuca eddy, a stagnant  
 20 region of water that occupies the shelf where it abruptly widens just north of the Strait of  
 21 Juan de Fuca.

22 Here we present intensive sampling of the Juan de Fuca eddy region. The observations  
 23 show the eddy is low in oxygen, and we find has undergone substantial vertical and lateral  
 24 mixing. This indicates that the waters have a surprisingly long residence time for a coastal  
 25 feature, and that this region extends the depth of the water column. In contrast to previous  
 26 literature we find that the water likely has low oxygen from being used for respiration rather  
 27 than being pulled from deep in the California Undercurrent.

28 The sampling also shows a remarkable flow separation of the equatorward shelf current  
 29 The current is shown to detach and is pushed offshore. Such events are readily seen in  
 30 satellite imagery, but the results here indicate that the separation extends the depth of the  
 31 water column on the shelf, and that this separation may be partially driven by the local  
 32 bathymetry. The separation is a very strong cross-shelf exchange event, and likely transports  
 33 substantial nutrient-rich coastal water offshore to drive productivity in the deeper ocean  
 34 adjacent to the continental slope.

35 **1 Introduction**

36 Cross-shelf exchange is important to the health and productivity of continental shelf re-  
 37 gions, where oxygenated water is exchanged with nutrient-rich, but oxygen-depleted nearshore  
 38 water. Cross-shelf transport usually requires ageostrophic flow, since balanced flow will tend  
 39 to follow topographic contours, often providing a barrier to lateral exchange (Brink, 2016).  
 40 Mechanisms for cross-shelf exchange include internal waves and instabilities in shelf-break  
 41 fronts. Most-dramatically, however, topography can drive cross-slope exchanges, often seen  
 42 most clearly in surface imagery, but occasionally observed *in-situ* (Barth et al., 2000).

43 Here we present detailed observations from the southern Vancouver Island shelf, col-  
 44 lected in summer 2013, and sampled with a rapid profiling vehicle equipped with a CTD  
 45 and oxygen sensor, supplemented by traditional hydrographic surveys. The shelf has com-  
 46 plicated bathymetry figure 1, with a somewhat typical shelf poleward of our study site, but  
 47 then widening in the lee of La Perouse Bank, and then hitting the Juan de Fuca canyon,  
 48 equatorward. Water from the strait of Juan de Fuca flows poleward as a buoyant current  
 49 that hugs the coast (Thomson et al., 1989; Hickey et al., 1991), while shelf water flows  
 50 equatorward in the summer under upwelling conditions, both forced by local winds and  
 51 via tele-connections with the long, homogenous shelves equatorward off Washington and  
 52 Oregon (Hickey et al., 1991; Thomson & Krassovski, 2015; Engida et al., 2016). Trapped  
 53 between these two currents is a region of relatively homogenous water that has been termed  
 54 the “Juan de Fuca” eddy (Freeland & Denman, 1982; Freeland & McIntosh, 1989; Foreman  
 55 et al., 2008; MacFadyen & Hickey, 2010).

56 One of our findings below is that the water in the deep pool of the Juan de Fuca  
 57 eddy is either quite old or undergone significant vertical mixing. The low oxygen found in  
 58 the Juan de Fuca eddy has caused it to be inferred to be upwelled from as deep as 400 m  
 59 (Freeland & Denman, 1982; Dewey & Crawford, 1988). This inference was based on the  
 oxygen being conservative, and hence having to come from close to the oxygen minimum

61 zone found further offshore (Mackas et al., 1987). This lead to hypotheses that perhaps the  
 62 eddy was fed by waters being drawn up a spur canyon of the Juan de Fuca canyon (called the  
 63 Spur Canyon) via ageostrophic transport from offshore to onshore due to the low pressure in  
 64 the eddy center (Weaver & Hsieh, 1987). Below, we will argue that there is not substantial  
 65 evidence of such transport, and that oxygen is likely low because of consumption due to  
 66 respiration.

67 A second important finding is that the water flowing equatorward along the shelf from  
 68 upstream all detaches from the shelf and is pushed offshore to be replaced by offshore water  
 69 that floods the southern shelf. Such events are important as they tend to transport nutrient  
 70 rich shelf water out into the open ocean, fueling offshore ecosystems. Similar offshore motion  
 71 has been remarked in the region using satellite images (Ikeda & Emery, 1984; Thomson &  
 72 Gower, 1998), and observed further to the south off Cape Blanco (Barth et al., 2000),  
 73 and other coasts (Relvas & Barton, 2005, e.g.). Net cross-shore transport of nutrients  
 74 and chlorophyll have been found in hydrographic surveys off Vancouver Island (Mackas  
 75 & Yelland, 1999), and associated with mesoscale features both in geostrophic velocities,  
 76 and in satellites. The mechanisms driving such separations are poorly understood, but  
 77 hypotheses include coastal hydraulics (Dale & Barth, 2001) leading to along-shore trapping  
 78 of coastal waves, wind stress curl variations (Castelao & Barth, 2007), induced relative  
 79 vorticity due to stretching of parcels that inertially overshoot their initial isobaths due to  
 80 a sudden change in downstream bathymetry, and the non-linear breaking of large-scale  
 81 meanders due to baroclinic instability between the wind-driven current and the California  
 82 Undercurrent (Ikeda et al., 1984; Batteen, 1997).

83 In this paper we present observations from 2013 (section 2), presenting the data in  
 84 a number of ways to highlight the important processes, with a focus on the offshore side  
 85 of the eddy region (section 3) where we consider the age of the eddy, the steadiness of the  
 86 front separating the eddy and the offshore water, properties along the spur canyon that  
 87 was believed to feed the eddy, and finally describe the large offshore separation of the shelf-  
 88 break current and its intrusion into the interior. We discuss the origin of the eddy and the  
 89 implications of the separating jet (section 4).

## 90 2 Site and Methods

91 Observations from three summer cruises in 2013 are discussed here. Two were hydro-  
 92 graphic surveys carried out on the *CCGS Tully*, one in June, and the other in late  
 93 September. The third was a finescale survey made in the Vancouver Island shelf between 21  
 94 and 30 August 2013, aboard the *R/V Falkor*. The study site was the southern portion of the  
 95 Vancouver Island Shelf (figure 1a), a particularly complicated region due to the bathymetry  
 96 and varied forcing.

97 At the south end of the study site is the Juan de Fuca canyon, which feeds dense water  
 98 into Juan de Fuca Strait. This dense water is mixed with fresh water from the Fraser River  
 99 at the sills and archipelagos further inland, and fluxes out the Strait again, where it turns  
 100 poleward along Vancouver Island to form the Vancouver Island Coastal Current. The Juan  
 101 de Fuca Canyon has a notable spur canyon (Spur Canyon), that incises the shelf towards  
 102 the north into the study site (figure 1b). The rest of the shelf is punctuated by a series of  
 103 banks and shallow basins. Notable is La Perouse bank, running along the shelf from the  
 104 north, and moving isobaths offshore until it abruptly ends at around 48.5 N. The shelf break  
 105 is characterized by a series of submarine canyons, in particular Nitnat Canyon and Barkley  
 106 Canyon.

107 Observations from the LB and LC lines were collected aboard the *CCGS Tully* from  
 108 2013-05-30 to 2013-05-31, which we will call “June”, and 2013-09-07 to 2013-09-09, which  
 109 we will call “September”. These lines span the depths from about 50 m to deep offshore.  
 110 The data comes from a lowered Seabird 9-11 CTD, with an SBE 43 oxygen sensor. Oxygen

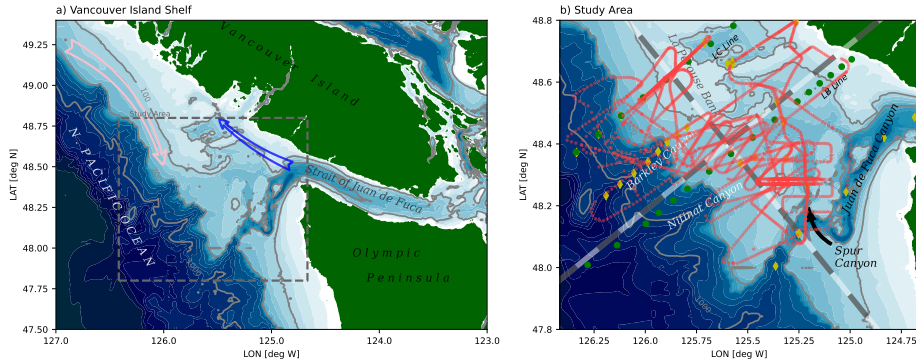


**Figure 1.** a) Study site on the Vancouver Island Shelf. The blue arrow indicates the direction of the Vancouver Island Coastal Current. The pink arrow indicates southward flow of the coastal upwelling current. The dashed box indicates the approximate limits of the study area. b) The study area with hydrographic casts from the La Perouse cruises along the LB and LC Lines are green dots, hydrographic casts during the Falkor cruise indicated in yellow dots, and Moving Vessel Profiler casts as red dots. The coordinate system used for this paper is shown with alternating grey and white bands at 10-km intervals.

111 data have been checked against bottle casts, and the CTD corrected for sensor offsets and  
112 thermal lags.

113 Observations aboard the *R/V Falkor* were carried out from 2013-08-21 to 2013-08-30,  
114 starting two weeks before the September *Tully* cruise. Data were collected with an ODIM  
115 Brooke-Ocean Moving Vessel Profiler, profiling to 200 m. The MVP was equipped with an  
116 AML Oceanographic CTD, and a Rinko Oxygen sensor with a 7-s response time foil. The  
117 MVP profiles at vertical fall speeds of  $3 \text{ m s}^{-1}$  to depths of 200 m or to within 5 m of the  
118 seafloor, whichever is shallower. Data collection took place while the ship cruised at speeds  
119 between 5 and 8 kts, usually at around 6 kts to enable fine horizontal spacing of the casts,  
120 with typical spacing less than 800 m. Data is collected during down- and up-casts, but is  
121 only reported for down-casts because the path through the water is highly asymmetric on  
122 the up-cast, whereas the downcast is largely vertical. The rapid speed of the profiling makes  
123 the oxygen measurements somewhat coarse, and probably biased due to the phase lag of  
124 the sensor, so we treat these largely qualitatively in this paper.

125 Unfortunately, neither vessel had an operational acoustic Doppler profiler during the  
126 cruises with which to make current measurements.

127 Winds during the cruises were typical for the west coast of Vancouver Island, with  
128 upwelling favorable winds during July and early August (figure 2). During the cruise, and  
129 for the week previous, the winds were intermittently downwelling favorable. Note that this  
130 locale is strongly affected by coastally trapped waves from further south, so doming of near-  
131 bottom isopycnals often persists despite local wind forcing (Thomson & Krassovski, 2015;  
132 Engida et al., 2016), and takes a finite amount of time to spin down.

### 133 3 Observations

#### 134 3.1 Early and late summer broad-scale surveys

135 Hydrographic sections along the LB and LC lines highlight summer conditions on the  
136 Southern Vancouver Island Shelf, and indicate some of the features we are focusing on in this  
137 paper (figure 3). During both cruises and at both lines there is clear evidence of upwelling,

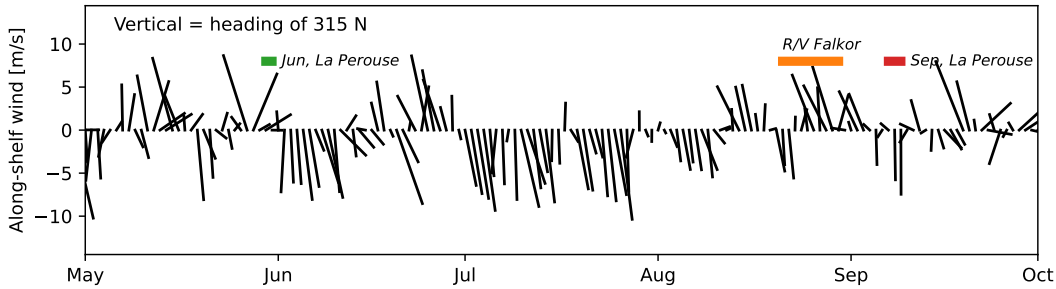


**Figure 2.** Wind from the La Perouse buoy (DFO, 2022). The vertical direction is along-shelf (chosen as a heading of 315 N). The wind components has been low-pass filtered to one-day averages. The timing of the cruises discussed in the paper are shown as colored bands.

138 with the  $26.4 \text{ kg m}^{-3}$  isopycnal reaching from 130 m to shallower than 85 m over the shelf.  
 139 This dense water tends to be low in oxygen and cool. Further onshore, isopycnals tilt back  
 140 down, and warm water fills the water column, evidence of the Vancouver Island Coastal  
 141 Current that hugs the coast here.

142 The “Juan de Fuca Eddy” region is along the LB Line, mostly inshore of 0 km. This  
 143 water is cooler and lower in oxygen than along the same isopycnal further offshore. Also  
 144 note that during the June cruise the water in this region was cooler and more oxygenated  
 145 than later in the summer during the September cruise. Near the surface, the isopycnals are  
 146 domed, but the low-oxygen anomaly extends as high as the thin surface mixed layer.

147 In contrast, the water upstream, along the LC line, does not show as much drawdown  
 148 of oxygen, and is somewhat warmer, at least offshore of La Perouse bank (figure 3 top three  
 149 rows). Water does not appear to make it over La Perouse bank into the basin onshore, or  
 150 if it does, it does so intermittently. There appears to be some mixing of the deeper water  
 151 and shallow water near  $26.4 \text{ kg m}^{-3}$ , with the water along this isopycnal becoming cooler  
 152 and lower in oxygen where it intersects the shelf.

153 The  $\theta-S$  properties show many of the features demonstrated above (figure 4a). Below  
 154  $26.6 \text{ kg m}^{-3}$  or so, the deep water masses are found offshore, and are largely homogenous.  
 155 Shallower, there are distinct differences between the water found on the shelf and water  
 156 found more offshore. These anomalies are hard to parse directly, so in this paper we use a  
 157 spice anomaly, relative to a straight line in  $\theta-S$  space (figure 4). The line passes the points  
 158  $7.75^\circ\text{C}, 30 \text{ psu}$  and  $6.6^\circ\text{C}, 35 \text{ psu}$ , and spice anomaly for a given water sample at density  
 159  $\sigma_\theta$  is  $\gamma = \alpha(T - T_0(\sigma_\theta)) + \beta(S - S_0(\sigma_\theta))$  where  $T_0(\sigma_\theta)$  and  $S_0(\sigma_\theta)$  are the temperature  
 160 and salinity along the mixing line at the same density as the water sample, with the sign  
 161 convention that positive is warmer and saltier than data along the mixing line. It is hard  
 162 to see from the  $\theta-S$  plot in figure 4, but this mixing line is a strong feature of the water  
 163 masses discussed in this paper.

164 The spice anomaly defined this way is mapped in the middle row of each set of plots in  
 165 figure 3. Offshore water tends to be high is absolute spice anomaly, with a positive-anomaly  
 166 layer (red) centered at  $26.4 \text{ kg m}^{-3}$  sandwiched between negative-anomaly layers above and  
 167 below. On the shelf ( $-10 \text{ km} < X < 30 \text{ km}$ ), the distinct  $\theta-S$  masses are attenuated and  
 168 much closer to the mixing line than the offshore water. Hugging the coast ( $X > 30 \text{ km}$ ), is  
 169 the Vancouver Island Coastal Current, with a negative spice anomaly in June, and a positive  
 170 anomaly in summer, consistent with the warming of this water during the summer.

171 The June and September cruises are quite similar in water properties, particularly in  
 172 the offshore waters. Water has upwelled from deeper depths in September, but has most

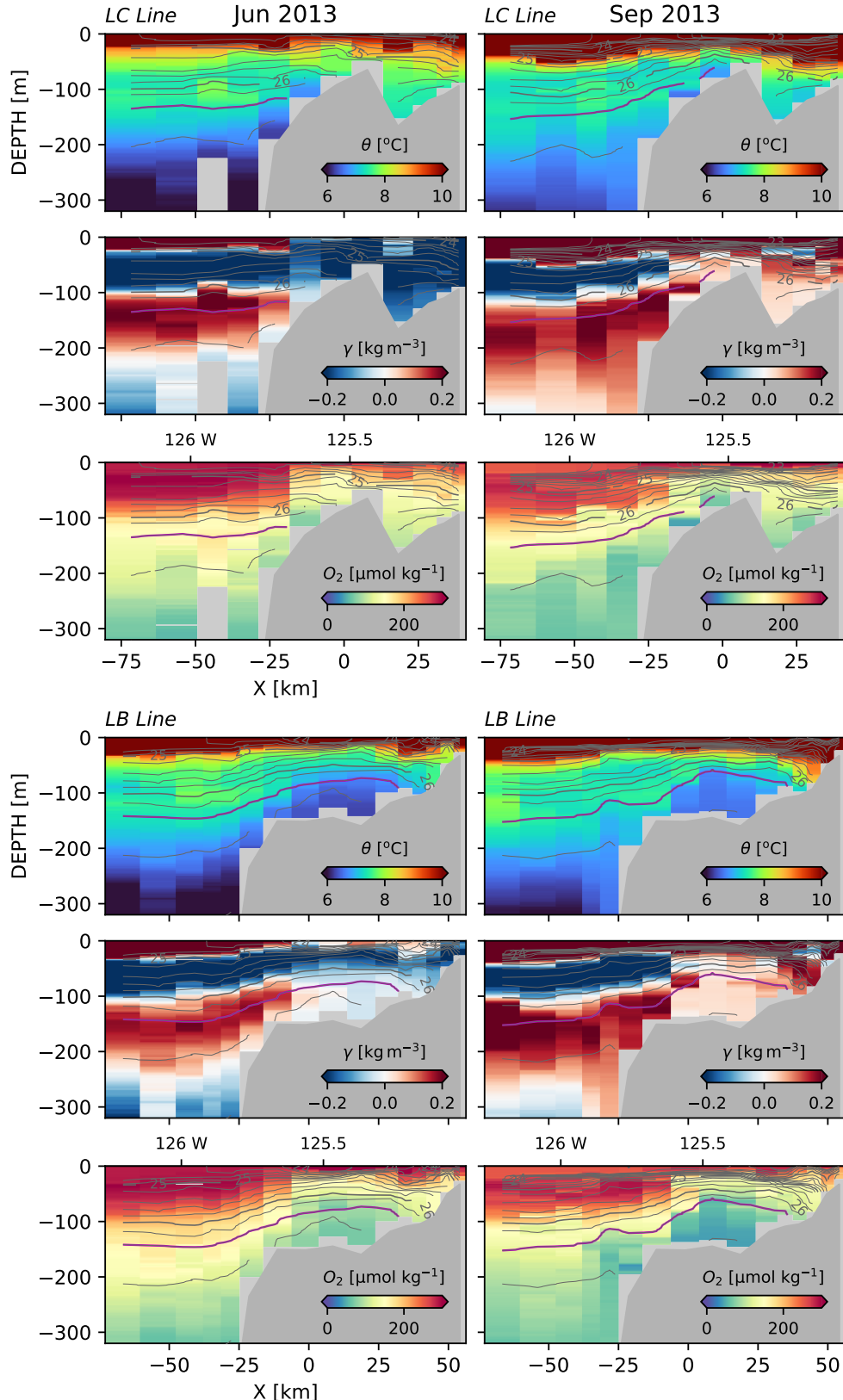


**Figure 3.** Observations along LC and LB lines in Jun and Sep 2013. X is across-shelf distance in the coordinate system shown in figure 1. Potential density is contoured every  $0.2 \text{ kg m}^{-3}$ , with the  $26.4 \text{ kg m}^{-3}$ . Potential temperature  $\theta$ , spice anomaly  $\gamma$  and oxygen concentration  $O_2$  are colored for each section.

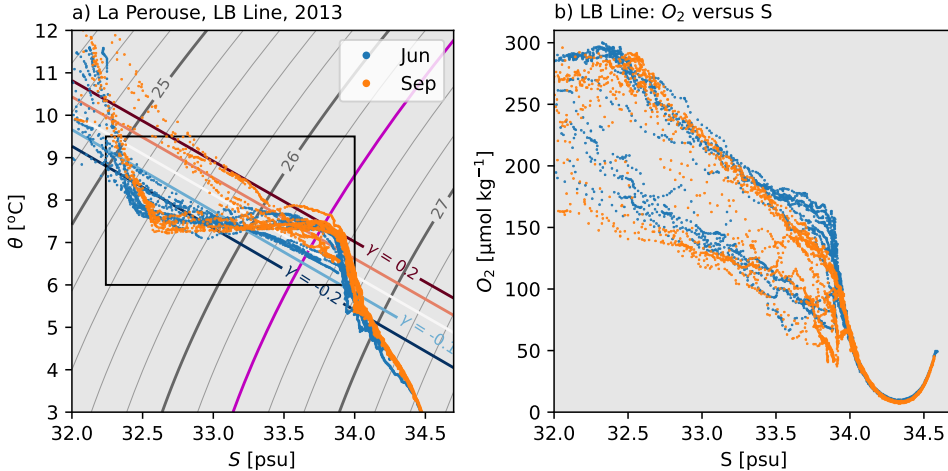


**Figure 4.** Potential temperature versus salinity for the La Perouse data shown in figure 3. Potential density is contoured in the same way. A definition of spice anomaly is shown in this plot, and discussed in the text. The rectangle is the  $\theta - S$  range used in figure 5 below.

of the same water mass characteristics as earlier in the year. The water on the shelf is somewhat warmer than earlier in the year, and by September has started to fall off the mixing line.

In terms of oxygen, both cruises have a similar dichotomy between the onshelf and offshelf water, with water found in the eddy tracking at least  $100 \mu\text{mol kg}^{-1}$  lower on the shelf than offshelf (figure 3, figure 4b). The very deepest water ( $S \approx 33.9$  psu) on the shelf shows a further  $50 \mu\text{mol kg}^{-1}$  drop between June and September along the LB line.

### 3.2 Fine-scale surveys

#### 3.2.1 Overview

As shown in figure 1, we conducted a large spatial survey of the shelf using the Moving Vessel Profiler, collecting over 2000 CTD casts in a relatively synoptic manner. This amount of data allows a reasonable census of the water masses that motivated our choice of the mixing line shown in figure 4. Binning in temperature and salinity, we can look at sample frequency of these observations figure 5, and we see that there are distinct water masses with few observations between them. Looking along the  $26.4 \text{ kg m}^{-3}$  isopycnal, we see that there is a large population along the mixing line. At the opposite extreme, we see that there is a large population with a positive spice anomaly of approximately  $0.2 \text{ kg m}^{-3}$ , representing the offshore water. Between these two end points there is a third water mass, somewhat indistinct from the offshore water mass, but very distinct from the water mass along the mixing line. These three water masses exist on deeper and shallower isopycnals as well, but become hard to distinguish from  $\theta - S$  properties alone as the properties converge near  $26.1 \text{ kg m}^{-3}$ .

These three water masses are quite coherent in space. While we did not do the specific La Perouse sections, our spatial coverage is such that we can make consistent synthetic sections (figure 6), taken at  $y = 42, 28, 14$ , and  $0 \text{ km}$  (see figure 1). During the August cruise, the upstream water along  $\sigma_\theta = 26.4 \text{ kg m}^{-3}$  has moderate spice anomaly of  $\gamma \approx 0.1 \text{ kg m}^{-3}$  (figure 6a), and in this representation, the water appears "pink". There is some higher-anomaly water offshore of  $x \approx -40 \text{ km}$  along this upstream section.

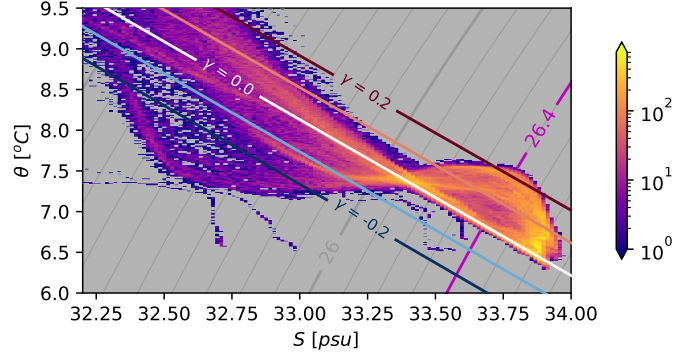


**Figure 5.** Sample density of salinity and potential density data from the cruise, with a logarithmic color scale. Grey contours are potential density relative to the surface, every  $0.1 \text{ kg m}^{-3}$ , and the magenta contour is the  $26.4 \text{ kg m}^{-3}$  isopycnal. Spice anomaly,  $\gamma$  is defined as temperature anomaly scaled by  $\alpha$  along isopycnals from the mixing line found in the well-mixed region onshore, in  $\text{kg m}^{-3}$ .

By  $y \approx 14 \text{ km}$ , this “pink” water along  $\sigma_\theta = 26.4 \text{ kg m}^{-3}$  is gone and is replaced by high spice anomaly water  $\gamma \approx 0.2 \text{ kg m}^{-3}$  (“red”) that is directly next to well-mixed water ( $\gamma \approx 0.0 \text{ kg m}^{-3}$ , “white”), a situation that persists further down the shelf (figure 6c, d). The onshore waters ( $-5 < X < 40 \text{ km}$ ) are remarkably well-mixed in  $\theta$ - $S$  space, despite still retaining significant density stratification.

Oxygen profiles, computed in the same manner, show similar trends, with the low-spice anomaly water clearly having a very low oxygen signature, while the strong negative spice anomaly shallower than  $\sigma_\theta = 26.4 \text{ kg m}^{-3}$  has very high oxygen, and the deeper water is also more oxygenated. Of note is that compared with the coarser sampling along the LC Line (figure 3), we see that there is a very abrupt transition between the low spice anomaly/low-O<sub>2</sub> water and the offshore water over the “Eddy” region. We will see below that this transition is even sharper than indicated by these synthetic sections, since they alias some lateral and temporal irregularity in the  $\theta$ - $S$ -compensated front.

The spatial patterns are very clear when considering a map-view of properties along the  $\sigma_\theta = 26.4 \text{ kg m}^{-3}$  isopycnal (figure 8). There is a region onshore of the south tip of La Perouse Bank (approximately 44.5 N, 125.75 W), that consists of water that is found along the mixing line (spice anomaly  $\gamma \approx 0 \text{ kg m}^{-3}$ ) with low oxygen saturations; this water is called the Juan de Fuca eddy (or Tully eddy), though here an eddy shape is not readily apparent. Offshore of this region is water that is very warm and salty in comparison ( $\gamma > 0.15 \text{ kg m}^{-3}$ ), and relatively high in oxygen (saturations of approximately 60%). The region between these two water masses is very abrupt, and is concave with respect to the isobaths on the shelf, stretching from La Perouse Bank to a shallow bank just above the Juan de Fuca canyon (48.3 N and 125.4 W).

Upstream of La Perouse bank, and Barkley Canyon, the water along the shelf has a weaker spice anomaly than the water further downstream ( $\gamma \approx 0.7$ , light pink colors). This water is also somewhat lower in oxygen than water from offshore, though not as depleted as the water in the “eddy”. This water appears to be pushed offshore just upstream of Barkley Canyon, and replaced on the shelf by the warmer offshore water.

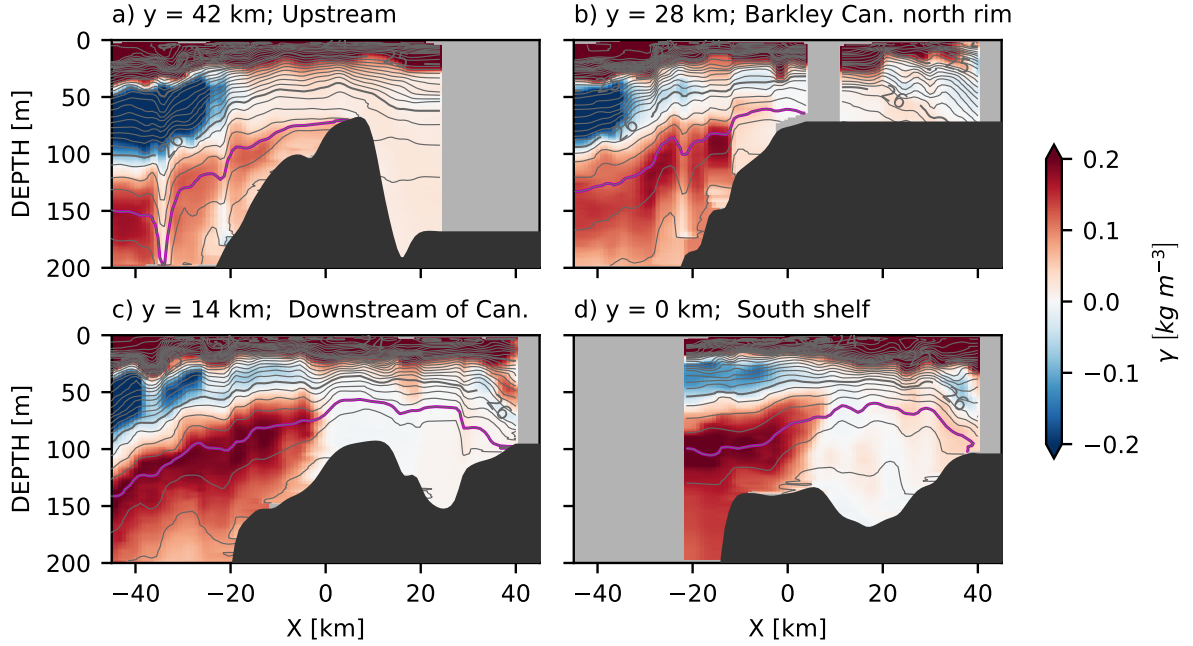


**Figure 6.** Synthetic sections of spice anomaly from the MVP data, projected along four lines from poleward (upstream of coastal current) a) to equatorward (downstream); the lines are shown in figure 1b). Isopycnals are contoured every  $\sigma_\theta = 0.2 \text{ kg m}^{-3}$ , with the  $\sigma_\theta = 26.4 \text{ kg m}^{-3}$  isopycnal highlighted in magenta. Colors are spice anomaly as defined in figure 5. "BC" in panel (c) refers to Barkley Canyon.

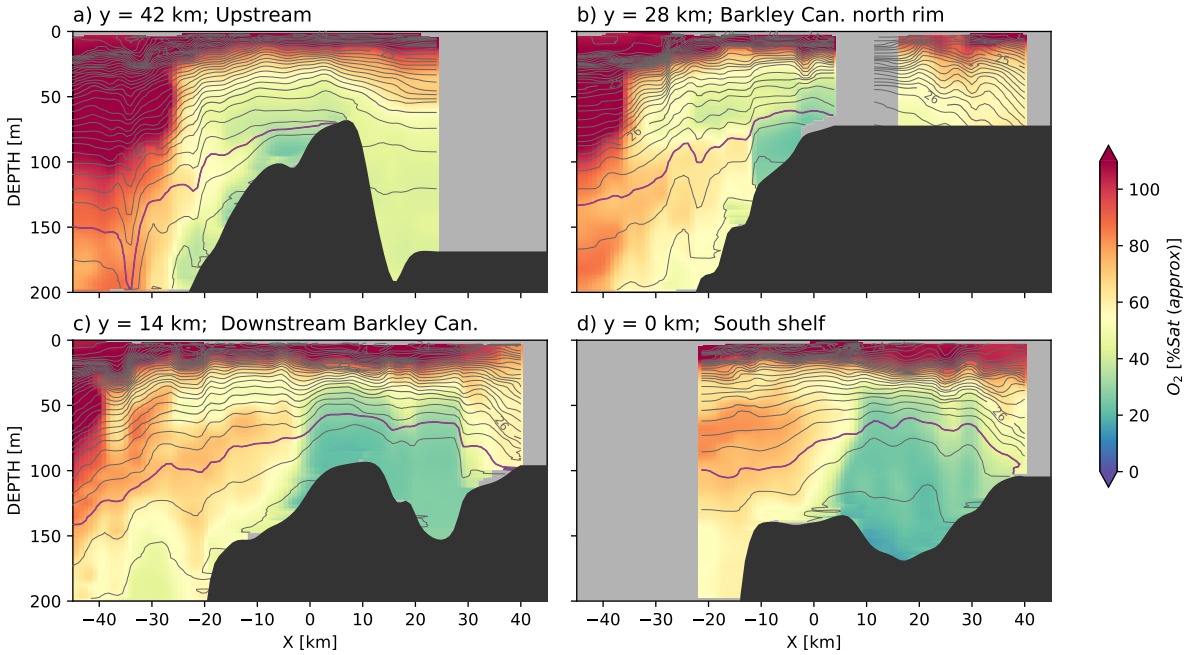


**Figure 7.** Synthetic sections of Oxygen, approximate percent saturation from the MVP data.

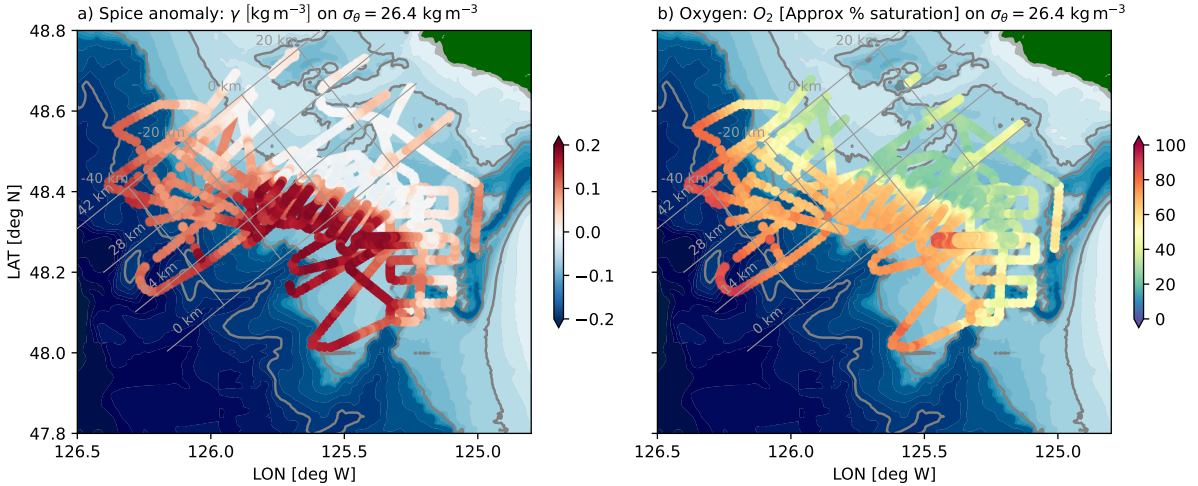


**Figure 8.** Spatial overview of a) local spice (temperature anomaly on an isopycnal: see text), and b) oxygen saturation on the  $\sigma_\theta = 26.4 \text{ kg m}^{-3}$  isopycnal. Grey cross-slope lines are cross sections indicated in figure 6. Along-slope grey lines are every 20 km in the cross-slope direction, with  $x = 0$  km near the 100-m isobath at the north end of the observation area.

229

### 3.2.2 Frontal survey

230  
231  
232  
233  
234  
235  
236

A systematic survey through the front between the offshore water and the “eddy” water demonstrates the structure of the front (figure 9). The survey started close to shore and passed through the Vancouver Island Coastal Current (casts 2030–2080). This water is buoyant and significantly fresher and cooler than water at the same density near the surface. There is strong evidence of isopycnal mixing of the surface water and the outflow water, with warm-salty water in the relatively wide front between the “eddy” water and the water in the current.

237  
238  
239  
240  
241  
242  
243  
244  
245  
246  
247

The front between the offshore water and the “eddy” water was passed through 10 times, showing its evolution following the along-shore equatorward flow. First, as noted in the composite sections, isopycnals slope up from offshore onto the shelf. This is in agreement with a shelf-break current, though the isopycnals flatten out in the “eddy” region. The front starts out very sharp, (along-track distance 50 km) though two small tendrils can be seen separating from the front on the inshore side. Similar tendrils are found on the second pass, perhaps a bit more separated from the front ( $\approx 80$  km), and on the third pass ( $\approx 95$  km). Note that these tendrils are made of up partially mixed water. The subsequent passes have more of this partially mixed water, such that the partially mixed region is up to 5-km wide by the fifth pass ( $\approx 150$  km). However, note that deeper isopycnals retain a sharp front, and indeed the front appears sharp again by the seventh pass at all depths.

248  
249  
250

There is evidence of some warmer water swirling into “eddy”, particularly along isopycnals deeper than  $26.4 \text{ kg m}^{-3}$ . Regions of warmer (and more oxygenated) water are found in tendrils at these depths (e.g.  $\approx 170$  km and  $\approx 185$  km).

251  
252  
253  
254  
255  
256

The overall effect is similar to what was seen in the Gulf Stream with similar observations (Klymak et al., 2016); there are two quite distinct water masses, as seen in the  $\theta$ - $S$  plot (figure 9c). There is only a small population of samples between these two, indicative of substantial isopycnal and vertical mixing, but even these populations are relatively cut off from the large water masses, indicating that they are well-mixed on their own, in short episodic events.

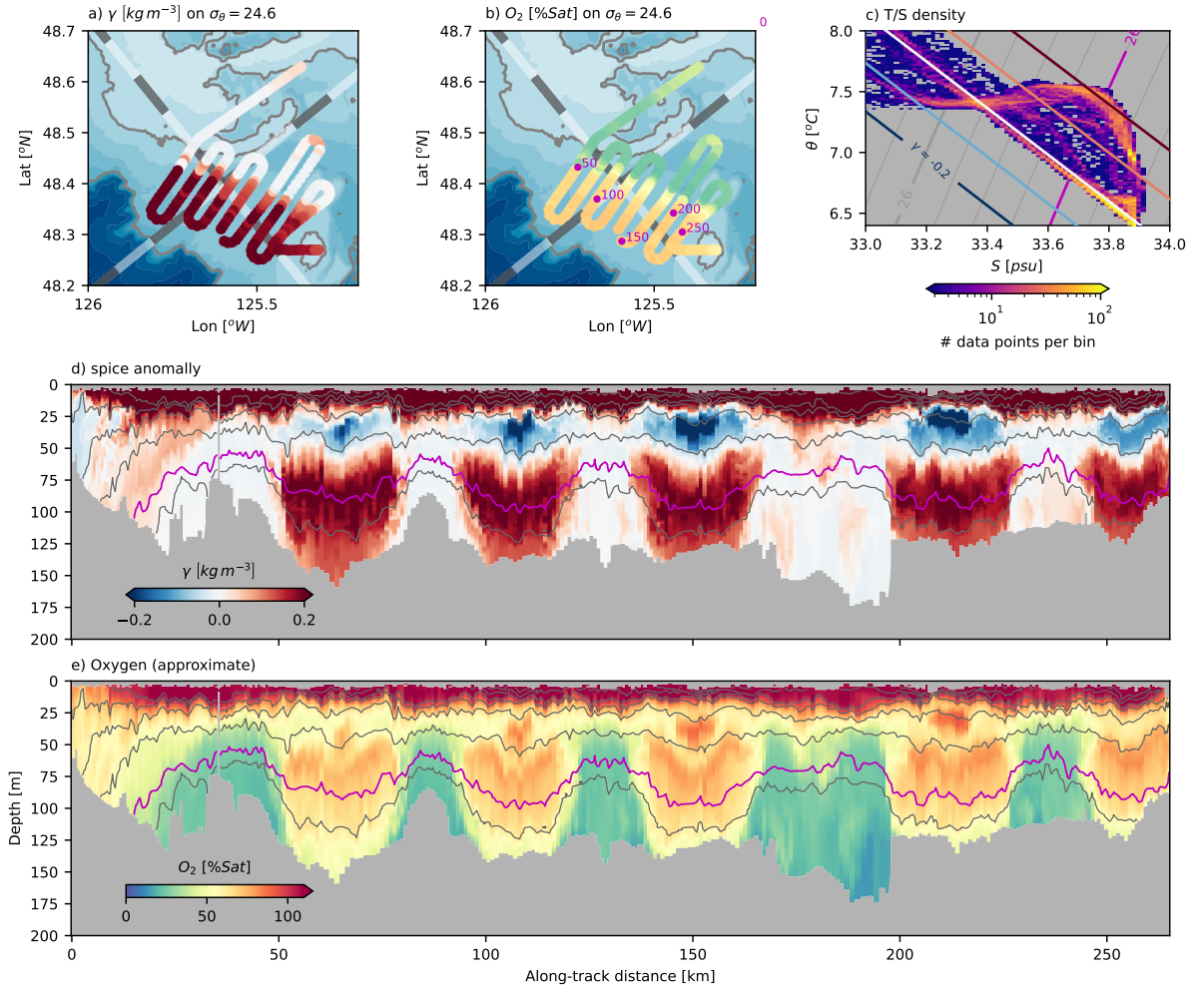


**Figure 9.** Data from a survey focusing on the front region (2013-08-28T15:11 to 2013-08-29T09:18) a) spice anomaly along  $26.4 \text{ kg m}^{-3}$ . Grey-white alternating lines are the coordinate system, with 10-km alternating shades. b) oxygen saturation; magenta dots correspond to distance along-track. c) density of data points (logscale) in this section of data. d) cross-section of spice anomaly along track. Grey isopycnals are contoured every  $0.5 \text{ kg m}^{-3}$ , and the  $26.4 \text{ kg m}^{-3}$  isopycnal is shown in magenta. e) cross-section of oxygen saturation.

257      **3.3 Spur Canyon**

258      The seasurface is low in the middle of the “Eddy”, so water has been hypothesized to  
 259      move up the Spur Canyon due to ageostrophic motion (Weaver & Hsieh, 1987; Freeland &  
 260      Denman, 1982). This is difficult to infer from water properties alone. Three transects up the  
 261      canyon indicate that deep isopycnals slope up into the canyon (figure 10, to approximately  
 262      30 km). Across the eddy, isopycnals are largely flat until they intersect the Vancouver Island  
 263      Coastal Current ( $x \approx 80$  km). The deeper isopycnals do not make it into the deeper basin  
 264      northeast of La Perouse bank ( $x \approx 70$  km).

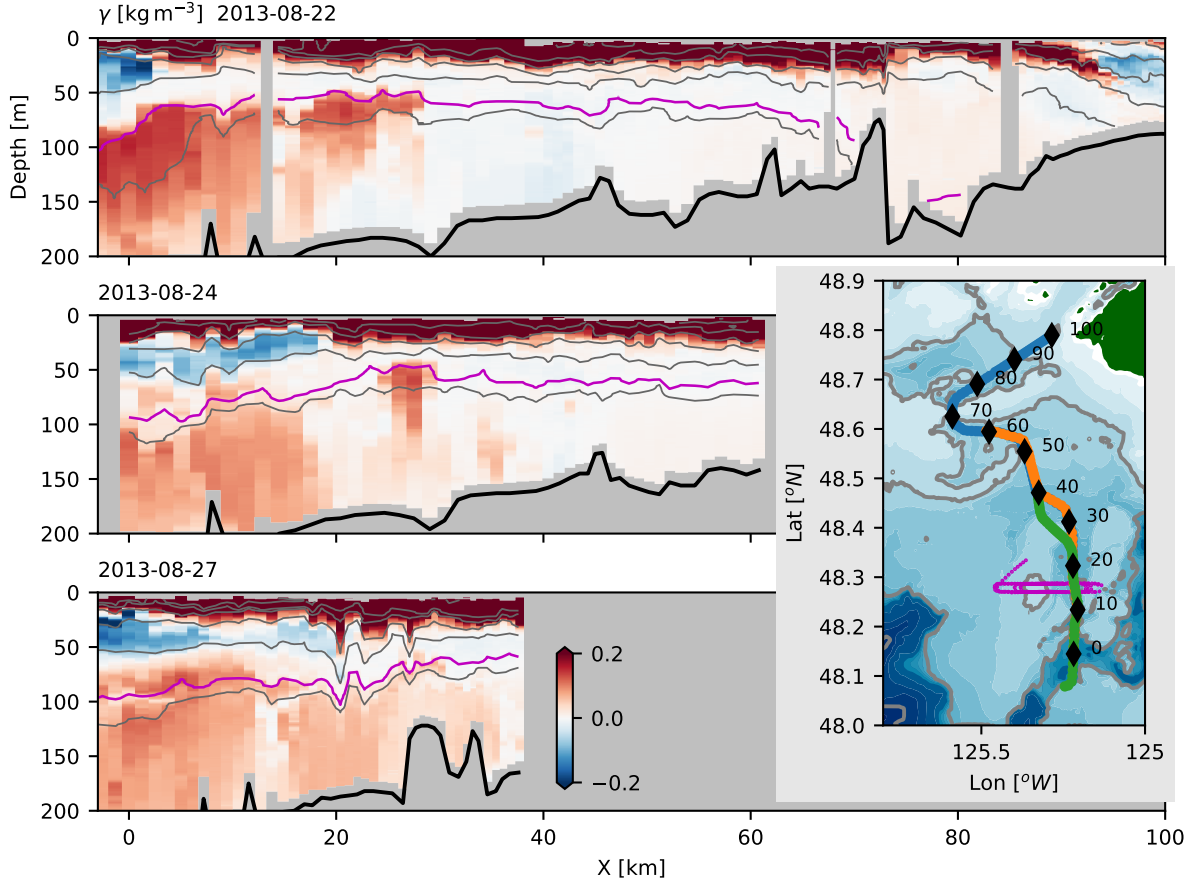


**Figure 10.** Magenta line in map inset is path taken during a cross-canyon survey.

265      Water properties along the canyon go from modified offshore water, to eddy water,  
 266      with a relatively consistent transition at about 30 km. Oxygen behaves in a similar manner,  
 267      though some of the incoming water has slightly lower oxygen than water inside the eddy  
 268      (not shown). Based on these sections, it is difficult to infer water motion up the canyon in  
 269      particular.

270      Much of the modified water in the Spur Canyon appears to come from the shelf to the  
 271      west, but heavily modified by tidal mixing. A repeated tidal survey over the bank on the  
 272      west side of the canyon shows a strong hydraulic response (figure 11) during onshore flow  
 273      (17:58–21:00). Note the tide here is largely diurnal, so this onslope flow only occurs once a  
 274      day. Given the stratification of  $N \approx 6 \times 10^{-3}$  rad s $^{-1}$  and an overturning scale of 50 m, we  
 275      might expect dissipation rates reaching  $\epsilon \sim L^2 N^3 \approx 5 \times 10^{-4}$  m $^2$  s $^{-3}$ , which is more than  
 276      three orders of magnitude higher than dissipation observed west of this location by (Dewey

& Crawford, 1988). The effect on the properties in the canyon is for water to spill over from the offshore front into the canyon during the tide. This water is rapidly mixed with surrounding water such that its strong offshore spice values are attenuated.

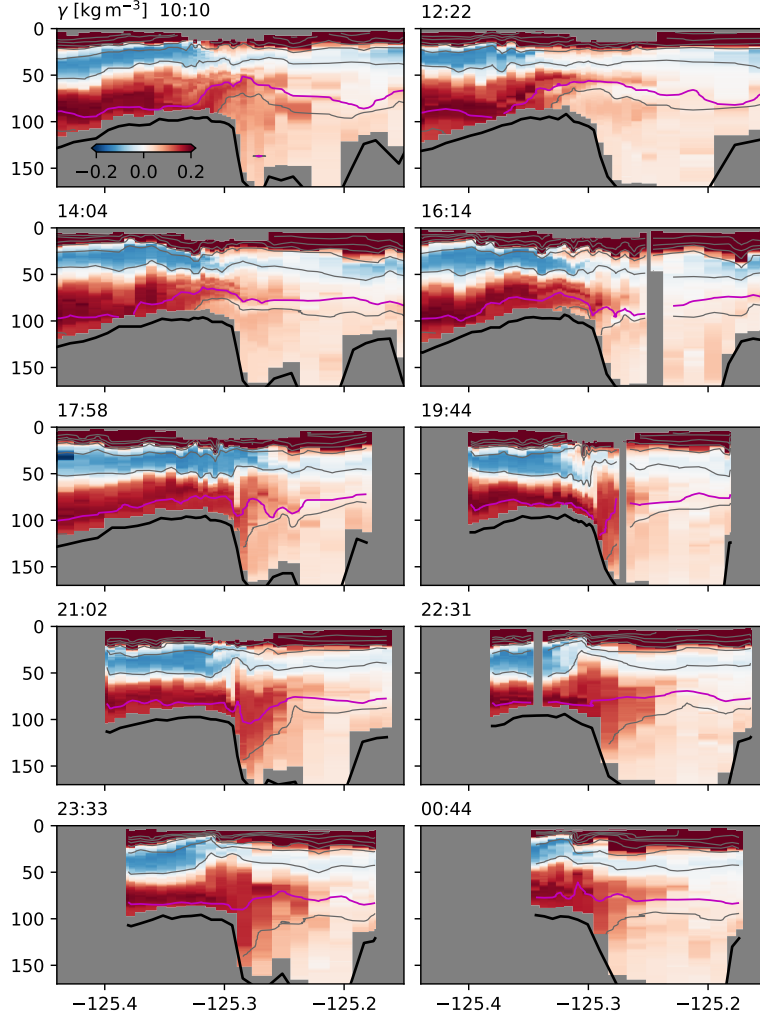


**Figure 11.** Repeated, tide-resolving survey across the Spur Canyon, time is indicated in the upper left of each plot (29 August, 2013).

This cross-canyon mixing makes it ambiguous if there is water moving up the canyon or not. There is indeed a general tendency along the canyon for higher spice water to be found offshore (figure 10) but it seems likely the source of the higher spice is over the bank rather than water being advected up the canyon.

### 3.4 Offshore tongue

The very narrow front on the offshore side of the “eddy” region persists, despite there being considerable “intermediate” water found upstream along the shelf. This water must go somewhere (or be accelerated unreasonably fast in the frontal region), and indeed it appears to largely be pushed offshore just upstream of Barkley Canyon (figure 12). There is a tongue of partially mixed ( $\gamma$  is pink along  $26.4 \text{ kg m}^{-3}$ ) that flows almost due south just west of 126 W. We had trouble crossing the whole tongue with the scale of our surveys, but it is at least

30 km wide. It also appears to end at approximately 48.2 N. This partially mixed water reaches from relatively shallow isopycnals to at least  $26.6 \text{ kg m}^{-3}$  (figure 12, left panel). Unfortunately, we cannot track the fate of the isopycnals deeper than this because they tilt down offshore, below the depth limit of the MVP. The shallower isopycnal appears to have the tongue closer to the shelf than at  $26.4 \text{ kg m}^{-3}$ , indicating strong three-dimensionality to this feature.

This feature is embedded in the larger scale isopycnal tilt caused by the upwelling (figure 12 right panels), so it is difficult to see dynamically what is driving this offshore push. One possibility is that it is simple flow separation as the water is not able to make the sharp turn around Swiftsure Bank. Whatever causes it, the water downstream is replaced by offshore water with much higher sigma values.

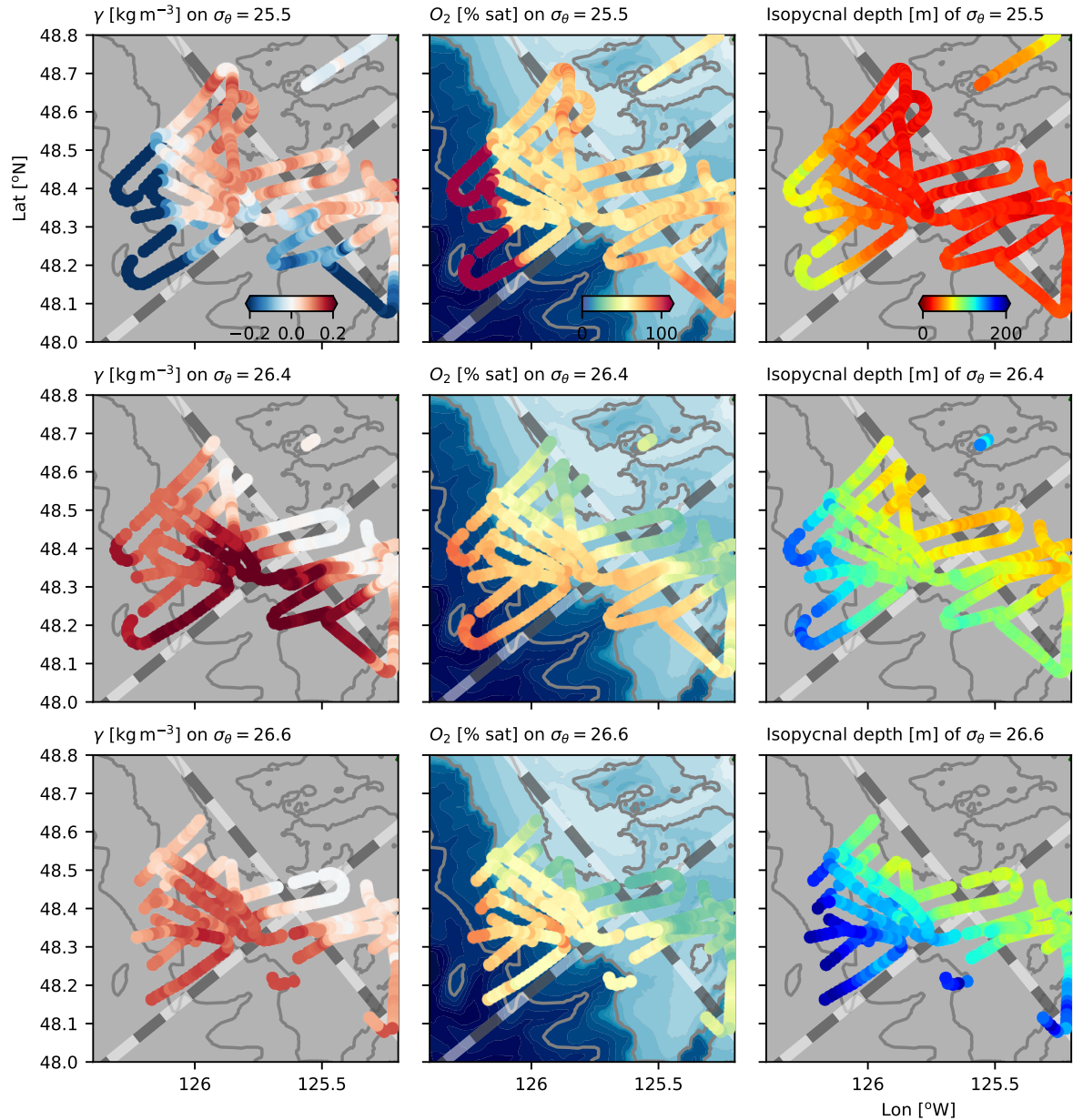


**Figure 12.**

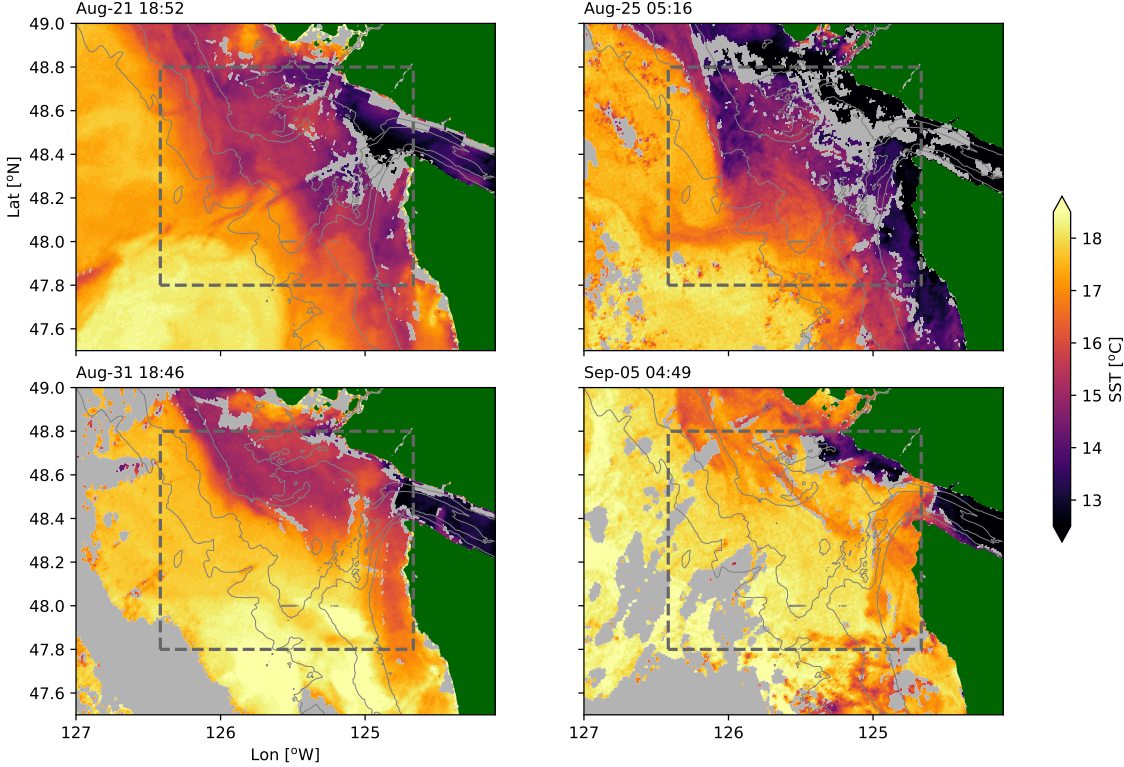


**Figure 13.** Sea surface temperature images from the observation period. Grey areas are clouds; dashed gray line is the study area. Depths are contoured in thin gray lines at 200, 150 and 100 m. (OSI SAF, 2015)

We can attempt to track this feature in satellite imagery, though there are lots of clouds during this time period. Sea-surface temperatures are generally colder coming out of the Strait of Juan de Fuca (figure 13). Water flowing equatorward along the shelf tends to be cooler than offshore water, though this water is significantly saltier than the Juan de Fuca water hugging the shelf. On Aug-25, there is a cold tongue of water separating from La Perouse bank, and pointing south at 125.8 W with a cooler tendril streaming west at 48 N. This feature is not as well-developed in the previous image, Aug 21, perhaps indicating that it is an evolving mesoscale feature. By 31 Aug, there is no surface expression of the feature, though tendrils of cooler water can be seen separating from La Perouse Bank. By Sep-05 the water gas significantly warmed, but the offshore pushing anomaly does not appear to have a surface signature.

Ccean chlorophyll estimates show the same feature (figure 14) demostrating the advection of a region of high chlorophyll to the west side of the eddy. It also shows a relatively high-chlorophyll squirt to the west, again exiting the study region at approximately 48 degrees N. The feature is relatively long-lived, on the order of one month. Inspection of images before 2013-08-05 were too obscured by clouds, or did not show this feature, and even by 2013-09-06 we see the feature fading from the satellite. However, note that this feature is somewhat south of tongue that we observe deeper in the water column, but is indicative of substantial offshore transport in the region.

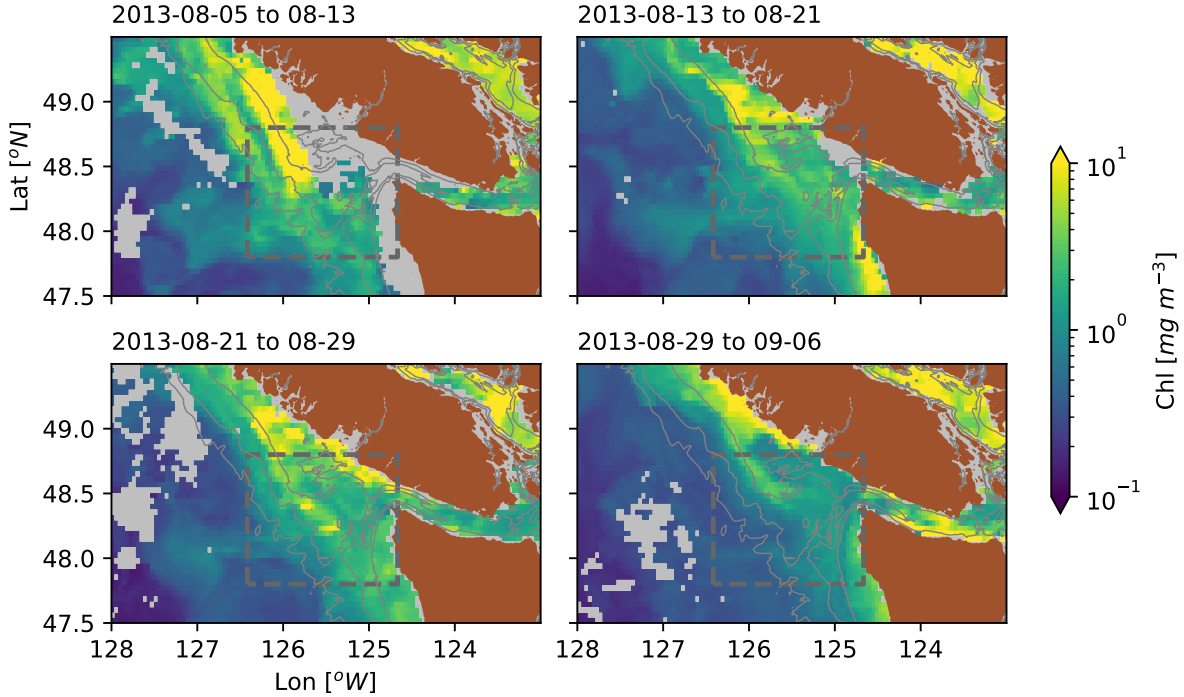


**Figure 14.** Surface chlorophyll density estimated from ocean color (Hu et al., 2012; NASA Ocean Biology Processing Group, 2017) over 8-day windows in 4-km bins. Gray regions had too many clouds for acceptable averages.

## 4 Summary and Discussion

The results of this fine-scaled survey perhaps pose more questions than they answer, but the questions are important to set the processes that should be looked for in understanding the circulation of the southern Vancouver Island shelf.

### 4.1 Age and source of the eddy water

The water we have been referring to as the Juan de Fuca Eddy is a relatively well-mixed water mass, as evidenced by the water therein lying along a mixing-line in  $\theta$ - $S$  space relative to water offshore (figure 4 and figure 5). Water coming equatorward along the shelf is closer to offshore water, though also shows clear signs of modification due to mixing.

Unfortunately, this data set cannot definitively track where the water in the eddy originated from. The deepest water in the eddy could originate along the  $\theta$ - $S$  line from approximately 5.5 degrees to 7.5 degrees (figure 4a), which in the open ocean spans depths from 420 m to 70 m. Mackas et al. (1987) attempted to determine the origin of the water by including oxygen as a third variable to resolve the ambiguous  $\theta$ - $S$  relation. However, as figure 4b makes clear, oxygen is definitely not a conserved property in the eddy, with concentrations up to  $150 \mu\text{mol kg}^{-1}$  lower in the eddy than the water found offshore, and in a way that definitely cannot result from conservative mixing. As a best guess, if the water in the deepest part of the eddy came from a vertical mixture of the water at  $26.5 \text{ kg m}^{-3}$  and an equal distance down in density space of  $26.7 \text{ kg m}^{-3}$ , then the deepest water in the eddy would be coming from a depth of 250 m. This is actually a relatively typical upwelling depth for coastal flows, and may not require extra input up Spur canyon as posited by Freeland and Denman (1982).

We found little evidence of vigorous flow up the Spur Canyon, or if there is, then the mixing in the canyon is quick enough to remove the  $\theta$ - $S$  signature of offshore water within 20 km (figure 10). We did find substantial evidence of mixing in the canyon, but the primary route of high-salinity water into the canyon appears to be due to tidal flow over the banks on the west side (figure 11), rather than evidence of flow up the canyon. However, it is also of note that upwelling winds had ceased at this point (figure 2), meaning that the offshore pressure gradient may be reduced, leading to less ageostrophic upwelling in the canyon. Whether the cessation of winds would also lead to a reduction of the low sea level height in the center of the eddy is an open question.

There is evidence of aging of the water in the eddy between late spring and late summer (figure 3), with a reduction of oxygen in the eddy. If we posited that the reduction was all from the same water, then the oxygen consumption rate over the time between the late-May and early September cruises would be on the order of  $0.5 \mu\text{mol kg}^{-1}\text{d}^{-1}$ . This seems on the low side of continental upwelling system estimates of apparent oxygen utilization rates, which are between 1 and  $5 \mu\text{mol kg}^{-1}\text{d}^{-1}$  (Dortch et al., 1994). So it seems possible the eddy has enough exchange with the surrounding water to have a shorter residence time.

There is partial mixing of the water in the eddy, though it remains vertically stratified, and the amount of homogenization is such that either the mixing is very strong, or the water is retained in the eddy for a long time. The amount of turbulence required to homogenize 100 m of water over 90 days is  $\kappa \approx 10^{-3} \text{ m}^2 \text{s}^{-1}$ . Given that the diffusivity implied in the cross-channel surveys was (very) locally on the order of  $\kappa_\rho = 10 \text{ m}^2 \text{s}^{-1}$ , this number is not outrageous if we think that such high dissipation is found in  $10^{-4}$  of the water column. We can more carefully quantify this by considering a synthetic profile of temperature and salinity based on an offshore profile, extrapolated from the bottom of the 200-m cast to 250 m, assuming that the temperature and salinity at 250 m are  $6.2 [\text{°C}]$  and 34 psu respectively (figure 15). Water at the offshore station was warmer than onshore, so the profile was also linearly interpolated to a surface value of (31.6 psu, 12 °C). The profile was then linearly compressed into a depth of 150 m representative of the shelf depth in the dense pool, and subjected to mixing with a constant diffusivity of  $\kappa = 10^{-3} \text{ m}^2 \text{s}^{-1}$ , with the surface and bottom values pinned under the assumption that the near-bottom source and surface waters are replenished from a large reservoir. Similar to the naive scaling, the T-S relationship does not approach a straight line until after approximately 60-100 days, or until the mixing affects a vertical length scale of  $\lambda = (\tau\kappa)^{1/2}$  that is greater than  $\approx 70 \text{ m}$ .

The sharpness of the front with the eddy and the offshore water is also intriguing. It was persistent for the duration of our detailed survey (figure 8), and, so far as we can tell with the limited resolution, was present during the La Perouse cruises. There is not any substantial bathymetry blocking the onshore incursion of water at this location, so there must be a dynamic barrier. In contrast, numerical simulations of this region reported by (Sahu et al., 2022) using a NEMO 36th-degree regional model indicate that there is relatively rapid exchange between the deep eddy water and the rest of the coastal ocean. In this model, the region where the eddy resides has velocities equal or greater than other parts of the shelf, and water has an approximate residence time of less than 20 days. Consequently, the eddy water does not develop a distinct  $\theta$ - $S$  signature from the surrounding water.

Overall, it would be an improvement to our understanding of the eddy if we could sample the shelf more persistently. The eddy was already well-formed by the June La Perouse cruise, and seems to evolve slowly during that time. Capturing its formation, presumably earlier in the spring, and its evolution through the year would be valuable in understanding retention and exchange on this productive part of the shelf.

## 4.2 Offshore exchange of shelf water

The (apparent) displacement of shelf water from La Perouse Bank is relatively dramatic. Eddies have been known to separate from irregular coastal topography, both at the

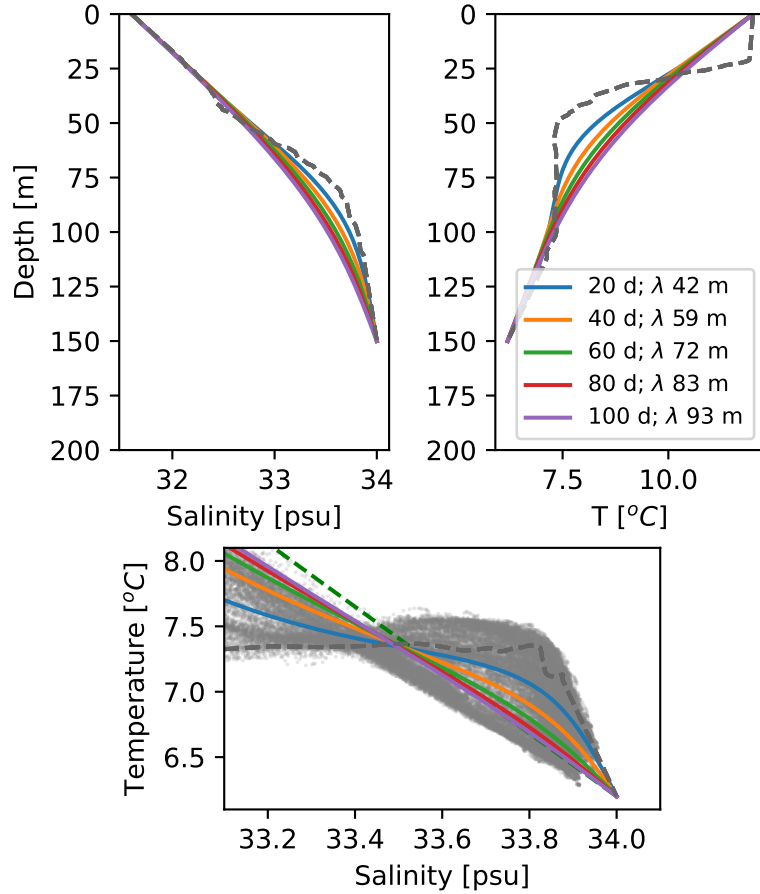


**Figure 15.** Mixing model assuming constant eddy diffusivity of  $\kappa = 10^{-3} \text{ m}^2 \text{s}^{-1}$  acting on an offshore temperature and salinity profiles compressed from 250 thick to 150 m thick. Profiles are pinned to the deep value at (34 psu, 6.2  $^{\circ}$ C), and a shallow one at (31.6 psu, 12  $^{\circ}$ C).

surface (Barth et al., 2000), and deeper in the water column (Pelland et al., 2013). It has been recognized that instabilities lead to exchange between the open ocean and the shelf at this location (Ikeda & Emery, 1984, 1984). However, observations of the wholesale replacement of shelf water by a new water mass from offshore, is relatively rare. In our situation it is clear that water from as deep as 150 m is separating from the shelf and moving offshore (figure 8, figure 12).

Satellite imagery makes it clear that there is often an exchange between coastal and deepwater along the Vancouver Island shelf (figure 16). Most years there are three or four large excursions from the shelf into the open ocean, many of them over 100 km long. The lengthscale in these images is somewhat larger than that inferred for this region by Ikeda et al. (1984). It is possible that there is even some spatial locking of these features, with a persistent separation at the north tip of the Island, and a strong tendency for one at 49.5 N. Our study area also has evidence of a squirt in most of the years, with 2011 being the only clear exception. General baroclinic instability of the upwelling front is a possible mechanism to drive offshore exchange (e.g. Ikeda et al., 1984; Durski & Allen, 2005), but this tends to be shallow, with smaller-scale instabilities that will not extend as far into the interior ocean as observed here. Rather it seems likely that the topographic change engendered by the sudden turn to the east of La Perouse bank catalyses a larger scale instability at this location. In Durski and Allen (2005), when including realistic shelf bathymetry including Heceta Bank, the region around the bank catalyzes intermittent large-scale instabilities similar to the feature here and along the coast (Battieen, 1997).

Large-scale mixing between the shelf and open ocean has been evident since the satellite era. Here we demonstrate that the flow is originating on the shelf and separating from the bathymetry and being injected into the interior down to the bottom of the water column. A similar observation was made by Barth et al. (2000) downstream of Cape Blanco, Oregon, where the coastal current was observed to detach from the shelf in the lee of the cape, and squirt into the interior. They hypothesized that as the current moved offshore, it deepened, stretching isopycnals and creating cyclonic relative vorticity that would tend to push the current back onshelf, but then it was caught in the undercurrent and stalled, being pushed offshore. It is also possible that coastally trapped waves in the region experience a hydraulic control, and these meanders are the response (Dale & Barth, 2001).

Regardless of the dynamics, the offshore transport is substantial. If we assume the coastal current is approximately  $0.1 \text{ m s}^{-1}$  over 100 m in the vertical and 20 km in the horizontal, it represents 0.2 Sv of nutrient- and chlorophyll-rich shelf water transported offshore. Our observations are a finer detailed representation of the kind of cross-shore transports inferred by Mackas and Yelland (1999) from hydrographic surveys, and definitively show that this water can originate from the shelf from relatively deep depths and be transported offshore. We do not have velocity measurements for the water that replaces it, but assuming that water also flows along-shelf, there is a large replacement of low-O<sub>2</sub>, low-nutrient water with offshore water at this location. This emphasizes the importance of three dimensional observations and modeling of cross-shelf dynamics when thinking about biological processes on the shelf.

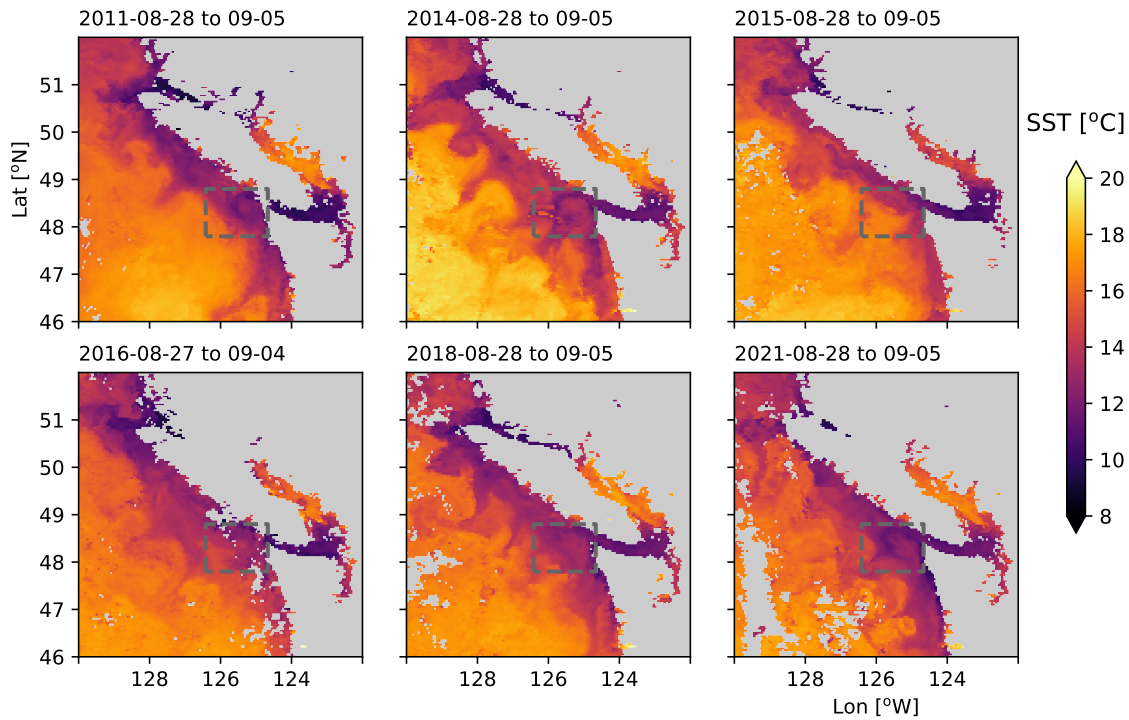


**Figure 16.** Late August sea-surface temperature, 8-day composites (NASA Ocean Biology Processing Group, 2019). From 2011 to 2021; missing years had too much cloud cover or no satellite coverage.

436 **Open Research**437 **Acknowledgments**

438 This section is optional. Include any Acknowledgments here.

439 **References**

- 440 Barth, J. A., Pierce, S. D., & Smith, R. L. (2000). A separating coastal upwelling jet at  
 441 Cape Blanco, Oregon and its connection to the California Current system. *Deep Sea*  
 442 *Res. II*, 47(5–6), 783 - 810. doi: [http://dx.doi.org/10.1016/S0967-0645\(99\)00127-7](http://dx.doi.org/10.1016/S0967-0645(99)00127-7)
- 443 Batteen, M. L. (1997, jan). Wind-forced modeling studies of currents, meanders, and  
 444 eddies in the california current system. *Journal of Geophysical Research: Oceans*,  
 445 102(C1), 985–1010. Retrieved from <https://doi.org/10.1029%2F96jc02803> doi:  
 446 10.1029/96jc02803
- 447 Brink, K. (2016). Cross-shelf exchange. *Annu. Rev. Mar. Sci.*, 8(1), 59–78. doi: 10.1146/  
 448 [annurev-marine-010814-015717](https://doi.org/10.1146/annurev-marine-010814-015717)
- 449 Castelao, R. M., & Barth, J. A. (2007, nov). The role of wind stress curl in jet separation  
 450 at a cape. *Journal of Physical Oceanography*, 37(11), 2652–2671. Retrieved from  
 451 <https://doi.org/10.1175%2F2007jpo3679.1> doi: 10.1175/2007jpo3679.1
- 452 Dale, A. C., & Barth, J. A. (2001, jan). The hydraulics of an evolving upwelling jet flowing  
 453 around a cape. *Journal of Physical Oceanography*, 31(1), 226–243. doi: 10.1175/  
 454 1520-0485(2001)031(0226:thoaeu)2.0.co;2
- 455 Dewey, R. K., & Crawford, W. R. (1988). Bottom stress estimates from vertical dissipation  
 456 rate profiles on the continental shelf. *J. Phys. Oceanogr.*, 18, 1167–1177.
- 457 DFO. (2022). *Marine environmental data section archive, buoy c46206*. Ecosystem and  
 458 Oceans Science, Department of Fisheries and Oceans Canada. Retrieved 2022-01-31,  
 459 from <https://meds-sdmm.dfo-mpo.gc.ca>
- 460 Dortch, Q., Rabalais, N. N., Turner, R. E., & Rowe, G. T. (1994, dec). Respiration  
 461 rates and hypoxia on the louisiana shelf. *Estuaries*, 17(4), 862. Retrieved from  
 462 <https://doi.org/10.2307%2F1352754> doi: 10.2307/1352754
- 463 Durski, S. M., & Allen, J. S. (2005). Finite-amplitude evolution of instabilities associated  
 464 with the coastal upwelling front. *J. Phys. Oceanogr.*, 35(9), 1606–1628. doi: 10.1175/  
 465 [jpo2762.1](https://doi.org/10.1175/jpo2762.1)
- 466 Engida, Z., Monahan, A., Ianson, D., & Thomson, R. E. (2016, oct). Remote forcing of  
 467 subsurface currents and temperatures near the northern limit of the california current  
 468 system. *J. Geophys. Res.*, 121(10), 7244–7262. Retrieved from <https://doi.org/10.1002/2016jc011880> doi: 10.1002/2016jc011880
- 469 Foreman, M., Callendar, W., MacFayden, A., Hickey, B., Thomson, R., & Di Lorenzo, E.  
 470 (2008). Modeling the generation of the Juan de Fuca eddy. *J. Geophys. Res.*. (in  
 471 press)
- 472 Freeland, H., & Denman, K. (1982). A topographically controlled upwelling ceter off  
 473 southern Vancouver Island. *J. Mar. Res.*, 40(4), 1069–1093.
- 474 Freeland, H., & McIntosh, P. (1989). The vorticity balance on the southern British Columbia  
 475 continental shelf. *Atmosphere–Ocean*, 27(4), 643–657.
- 476 Hickey, B., Thomson, R., Yih, H., & LeBlond, P. (1991). Velocity and temperature fluctua-  
 477 tions in a buoyancy-driven current off Vancouver Island. *J. Geophys. Res.*, 96(C6),  
 478 10,507–10,538.
- 479 Hu, C., Lee, Z., & Franz, B. (2012). Chlorophyll a algorithms for oligotrophic oceans: A  
 480 novel approach based on three-band reflectance difference. *J. Geophys. Res.*, 117(C1).  
 481 doi: 10.1029/2011jc007395
- 482 Ikeda, M., & Emery, W. J. (1984, may). A continental shelf upwelling event off vancouver  
 483 island as revealed by satellite infrared imagery. *J. Mar. Res.*, 42(2), 303–317. doi:  
 484 10.1357/00222408478502774
- 485 Ikeda, M., Mysak, L. A., & Emery, W. J. (1984, jan). Observation and modeling

- 487 of satellite-sensed meanders and eddies off vancouver island. *J. Phys. Oceanogr.*,  
 488 14(1), 3–21. Retrieved from <https://doi.org/10.1175%2F1520-0485%281984%29014%3C0003%3Aoamoss%3E2.0.co%3B2> doi: 10.1175/1520-0485(1984)014<0003:oamoss>2.0.co;2
- 491 Klymak, J. M., Shearman, R. K., Gula, J., Lee, C. M., D’Asaro, E. A., Thomas, L. N., ...  
 492 others (2016). Submesoscale streamers exchange water on the north wall of the Gulf  
 493 Stream. *Geophys. Res. Lett.*. doi: 10.1002/2015GL067152
- 494 MacFadyen, A., & Hickey, B. M. (2010). Generation and evolution of a topographically  
 495 linked, mesoscale eddy under steady and variable wind-forcing. *Continental Shelf  
 496 Research*, 30(13), 1387–1402.
- 497 Mackas, D. L., Denman, K. L., & Bennett, A. F. (1987). Least squares multiple tracer  
 498 analysis of water mass composition. *J. Geophys. Res.*, 92(C3), 2907–2918.
- 499 Mackas, D. L., & Yelland, D. R. (1999, nov). Horizontal flux of nutrients and plankton  
 500 across and along the british columbia continental margin. *Deep Sea Res. II*, 46(11-12),  
 501 2941–2967. doi: 10.1016/s0967-0645(99)00089-2
- 502 NASA Ocean Biology Processing Group. (2017). *MODIS-aqua level 3 mapped chloro-  
 503 phyll data version r2018.0*. NASA Ocean Biology DAAC. Retrieved from <https://oceancolor.gsfc.nasa.gov/data/10.5067/AQUA/MODIS/L3M/CHL/2018> doi: 10  
 504 .5067/AQUA/MODIS/L3M/CHL/2018
- 505 NASA Ocean Biology Processing Group. (2019). *MODIS-aqua level 3 mapped SST data  
 506 version r2019.0*. NASA Ocean Biology DAAC. Retrieved from [https://oceandata.sci.gsfc.nasa.gov/ob/getfile/AQUA\\_MODIS](https://oceandata.<br/>
  507 .sci.gsfc.nasa.gov/ob/getfile/AQUA_MODIS)
- 508 OSI SAF. (2015). *GHRSST level 2p sub-skin sea surface temperature from the Advanced  
 509 Very High Resolution Radiometer (AVHRR) on Metop satellites (currently Metop-A)  
 510 (GDS V2) produced by OSI SAF*. NASA Physical Oceanography DAAC. Retrieved  
 511 from [https://podaac.jpl.nasa.gov/dataset/AVHRR\\_SST\\_METOP\\_A-OSISAF-L2P-v1.  
 513 .0](https://podaac.jpl.nasa.gov/dataset/AVHRR_SST_METOP_A-OSISAF-L2P-v1.<br/>
  512 .0) doi: 10.5067/GHAMA-2PO02
- 514 Pelland, N. A., Eriksen, C. C., & Lee, C. M. (2013). Subthermocline eddies over the  
 515 washington continental slope as observed by seagliders, 2003-09. *J. Phys. Oceanogr..*  
 516 doi: 10.1175/JPO-D-12-086.1
- 517 Relvas, P., & Barton, E. D. (2005, jan). A separated jet and coastal counterflow during up-  
 518 welling relaxation off cape são vicente (iberian peninsula). *Continental Shelf Research*,  
 519 25(1), 29–49. Retrieved from <https://doi.org/10.1016%2Fj.csr.2004.09.006>  
 520 doi: 10.1016/j.csr.2004.09.006
- 521 Sahu, S., Allen, S. E., Saldías, G. S., Klymak, J. M., & Zhai, L. (2022, mar). Spatial and  
 522 temporal origins of the la perouse low oxygen pool: A combined lagrangian statistical  
 523 approach. *J. Geophys. Res.*, 127(3). doi: 10.1029/2021jc018135
- 524 Thomson, R. E., & Gower, J. F. R. (1998, feb). A basin-scale oceanic instability event in  
 525 the gulf of alaska. *J. Geophys. Res.*, 103(C2), 3033–3040. Retrieved from <https://doi.org/10.1029%2F97jc03220> doi: 10.1029/97jc03220
- 526 Thomson, R. E., Hickey, B. M., & LeBlond, P. H. (1989). The Vancouver Island Coastal  
 527 Current: Fisheries barrier and conduit. In R. J. Beamish & G. A. McFarlane (Eds.),  
 528 *Effects of ocean variability on recruitment and an evaluation of parameters used in  
 529 stock assessment models*. Fisheries and Oceans Canada.
- 530 Thomson, R. E., & Krassovski, M. V. (2015, dec). Remote alongshore winds drive variability  
 531 of the California Undercurrent off the British Columbia–Washington coast. *J. Geophys.  
 532 Res.*, 120(12), 8151–8176. doi: 10.1002/2015jc011306
- 533 Weaver, A. J., & Hsieh, W. W. (1987). The influence of buoyancy flux from estuaries on  
 534 continental shelf circulation. *J. Phys. Oceanogr.*, 17, 2127–2140.
- 535